Precipitation-elevation relationship: Non-linearity and space–time variability prevail in the Swiss Alps

Lionel Benoit, Erwan Koch, Nadav Peleg, Gregoire Mariethoz

▶ To cite this version:

Precipitation-elevation relationship: Non-linearity and space–time variability prevail in the Swiss Alps

ABSTRACT

The relationship between mean daily precipitation and elevation is often regarded as linear and positive, resulting in simple "precipitation lapse rate" equations frequently employed to extrapolate daily rainfall from a single weather station over a large area. We examine the precipitation-elevation relationship in the Swiss Alps using a combination of weather radar and rain gauge data to test this common assumption, challenging it by fitting a two-segment piecewise linear model with a mid-slope break-point as an alternative. By examining data stratified by catchment, season, and weather type, we assess the space–time variability of the precipitation-elevation relationship. We conclude that a non-linear and non-stationary model seems necessary to capture the variability of the observed precipitation-elevation relationship. Based on our findings, we suggest that the simplified precipitation lapse rate concept is misleading and should be reconsidered in hydrological applications, emphasizing the need for a more realistic representation of precipitation variability over time and space.

1. Main

1.1. The precipitation lapse rate: An over-simplification of orographic effects?

Orographic precipitation is conceptualized as a dynamic process in which a humid airmass is transported over mountains by large-scale circulations, resulting in adiabatic cooling, reduced pressure, and condensation that leads to precipitation (Roe, 2005; Houze, 2012). A natural consequence is that it tends, on average, to precipitate more in higher elevations than in lowlands along storm trajectories (Foresti and Pozdnoukhov, 2012), while lowlands on the other side of the ridge experience less precipitation (known as the "rain-shadow effect"; Siler et al., 2013). Consequently, many studies assume a determined positive relationship between mean daily precipitation and elevation, and they use linear precipitation lapse rates (Bohne et al., 2020; Dura et al., 2024). For example, precipitation lapse rates are routinely employed in catchment hydrological models to extrapolate precipitation from a measured gauging station to the rest of the catchment (Markstrom et al., 2015; Garavaglia et al., 2017), or to map precipitation from sparse rain gauge observations (Daly et al., 1994; Isotta et al., 2014).

However, relationships between precipitation and elevation are rarely observed systematically due to the paucity of precipitation data in high-elevation areas. When observed, precipitation-elevation relationships often differ from the simplified linear and positive relationship described above. In some cases, regional-scale synoptic conditions dominate over local altitudinal effects (Longman et al., 2021; Benoit and Sichoix, 2023). In others, very small-scale effects can locally change the measured precipitation amounts, such as peak rain rates overshooting the crest of mountains (Benoit et al., 2021) or localized convective rainfall (Michelon et al., 2021). In some cases, local inversions of the precipitation-elevation relationship have been observed and attributed to rain shadow effects (Collados-Lara et al., 2018) or the presence of the

trade wind inversion in the tropics (Giambelluca et al., 2013). Furthermore, the impact of elevation on precipitation depends on both the temporal scale and the precipitation feature of interest. For example, short-duration extreme precipitation has been shown to often decrease with elevation, resulting in a reverse orographic effect for high-intensity precipitation (Marra et al., 2022; Dallan et al., 2023). In fact, orographic precipitation is a complex phenomenon that depends on many intricated non-linear processes; therefore it has been argued that local discrepancies can be expected between the textbook explanation of orographic precipitation and actual precipitation (Masson and Frei, 2014).

1.2. Alternatives to the precipitation lapse rate model

We use a combination of radar and rain gauge data over the Swiss Alps to test whether the common assumption of a precipitation lapse rate (i.e., a linear and positive relationship between elevation and mean daily precipitation) holds for a mountain range of the mid-latitudes experiencing contrasting hydro-climates (Isotta et al., 2014; Panziera et al., 2018). We challenge this linear dependence model between precipitation and elevation with one of the simplest possible non-linear alternatives, namely a two-segment piecewise linear model with a mid-slope break-point. The variability of the precipitation-elevation relationship in space and time is assessed by performing the study on data stratified per catchment (Fig. 1a) and per seasonal weather types (Fig. 1b). The seasonal weather types are obtained by a statistical classification of daily pressure fields above Europe to delineate quasi-stationary states of the atmosphere (i.e., groups of days with similar atmospheric conditions). This classification was chosen as a basis for our analysis because it allows us to link the precipitation-elevation relationship with a discrete set of homogeneous atmospheric conditions. We explore the linearity, sign, and magnitude of the precipitation-elevation relationship by adjusting five competing regression models to the precipitation-elevation observation scatter plot (Fig. 1c).
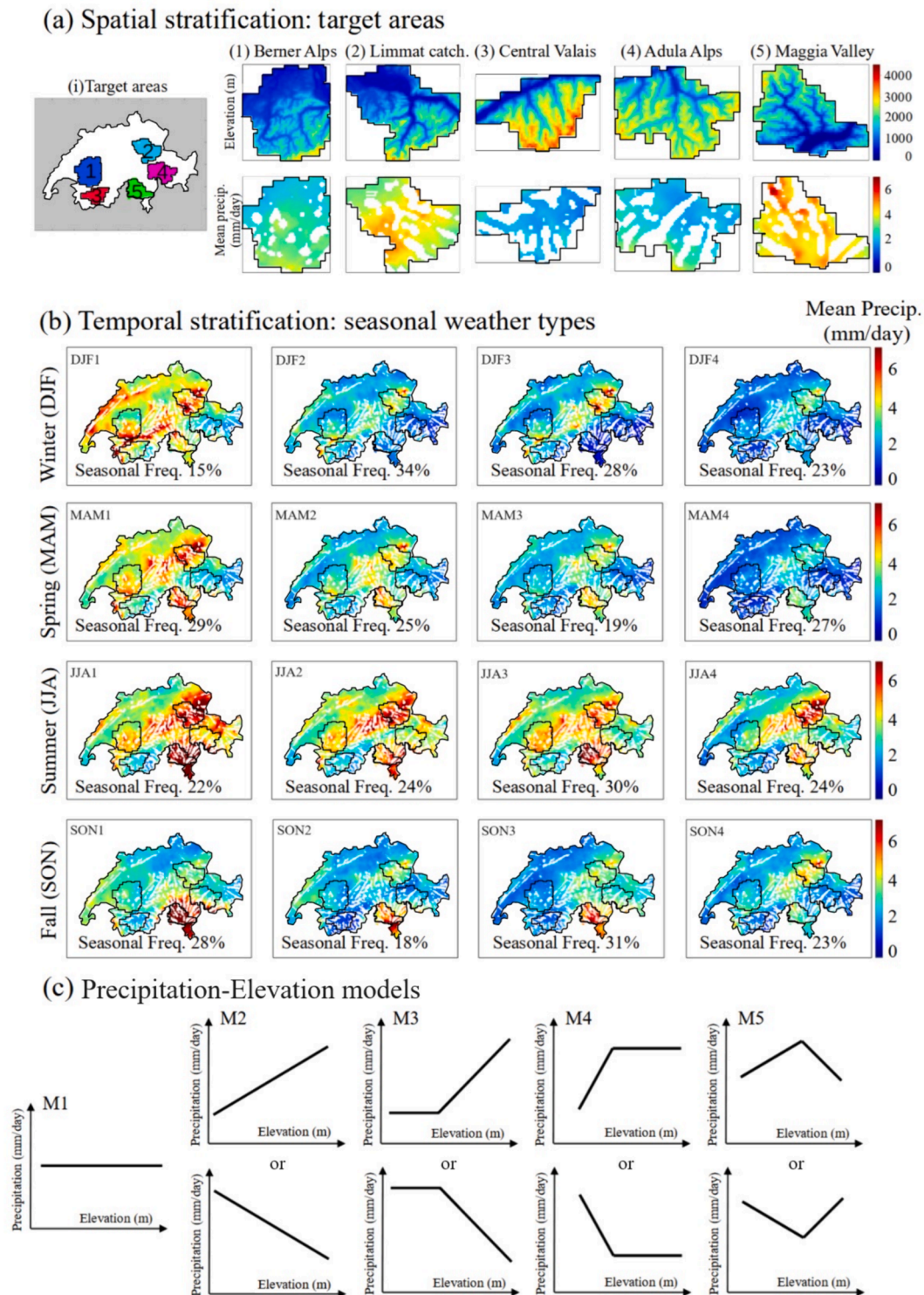
Fig. 1. Space-time stratification of the precipitation dataset and possible models of the precipitation-elevation relationship. a. Target areas. Left: location within Switzerland; right: topography (top) and mean annual precipitation (bottom). b. Seasonal weather types (4 seasons and 4 types per season; Yiou et al., 2008) and associated mean precipitation fields over all of Switzerland. Within each season, the weather types are ordered from the wettest (left) to the driest (right). The "Seasonal Freq." label denotes the frequency of occurrence of each weather type within the season of interest. c. Schematic view of the Precipitation-Elevation models used to test the linearity of orographic effects. In the precipitation maps in a. and b., the white pixels denote areas where precipitation data are considered unreliable and are therefore discarded from the analysis (see Fig. S1 for details).

1.3. Linear precipitation lapse rate in the Swiss Alps is the exception and not the rule

In the Swiss Alps, the sign, magnitude, and linearity of the influence

of elevation on mean daily precipitation vary tremendously in space and time (Fig. 2). Regarding the variability in space (i.e., comparing different curves within a single panel in Fig. 2), one can notice that for almost all 16 seasonal weather types, the selected model and the value of
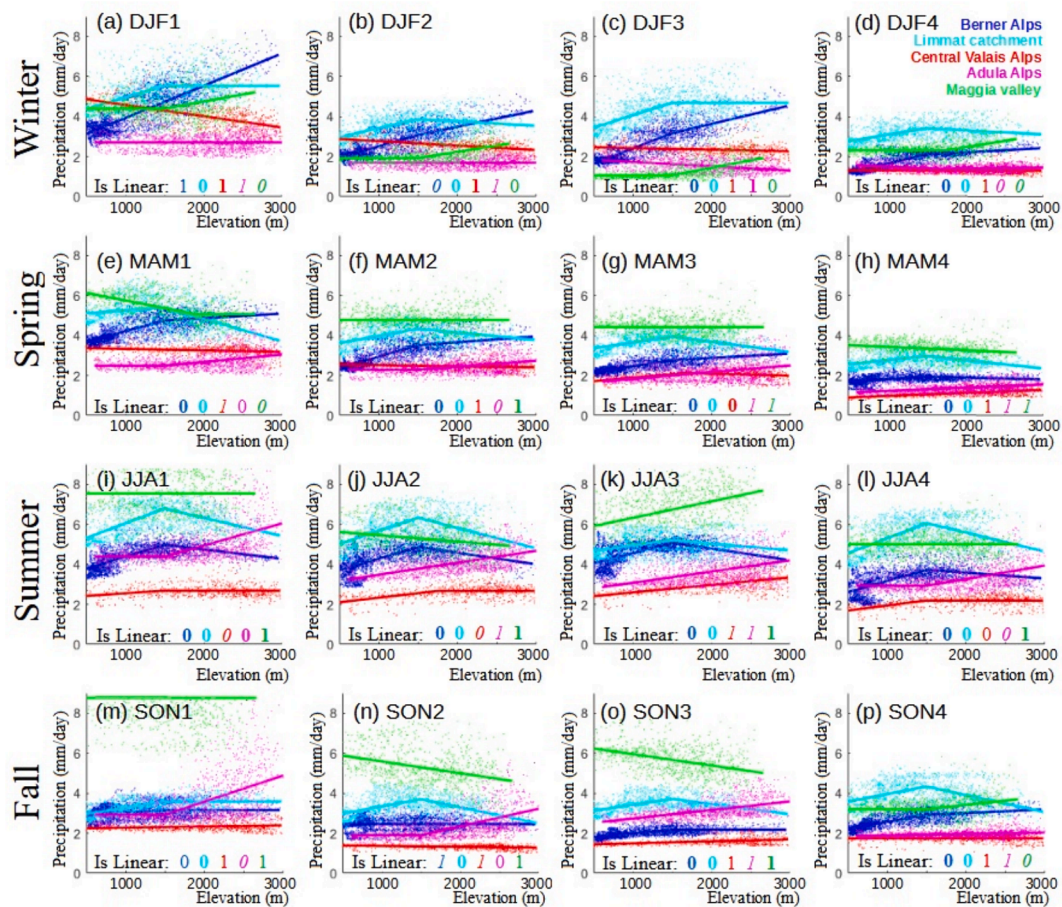
Fig. 2. Observed precipitation-elevation relationships (scatter plots) and adjusted models (solid lines) for all 16 seasonal weather types and 5 target areas considered in the study (blue: Berner Alps, light blue: upper Limmat catchment, red: central Valais Alps, pink: Adula Alps, green: Maggia Valley). The Is_Linear booleans at the bottom of each subplot denote if the selected model of precipitation-elevation relationship is linear (1) or non-linear (0). The font of the boolean informs if the evidence for the selected hypothesis of linearity is weak (italic), strong (normal font), or very strong (bold) (for details see Methods: Investigating the precipitation-elevation relationship).
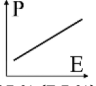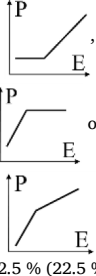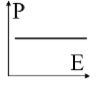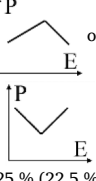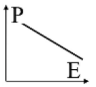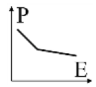
its parameters differ between areas. Regarding the temporal variability of the precipitation-elevation relationship (i.e., comparing curves with the same color between different panels in Fig. 2), one can notice that for a given area, the selected model and its parameters vary widely depending on the season and the weather type. Many interacting phenomena can explain these space–time variations of the precipitation-elevation relationship in response to changing weather types. As an illustration, the seasonal change in precipitation regime helps explain the different patterns of orographic effects observed between the external Alps (Berner Alps and Limmat catchment, in blue and light blue in Fig. 2) and the internal Alps (Central Valais and Adula Alps, in red and pink in Fig. 2) under the influence of westerly low-pressure systems (weather types DJF1–2 and JJA1–2). When winter stratiform precipitation prevails (Fig. 2a and b), the windward external Alps experience a positive precipitation-elevation relationship due to orographic precipitation enhancement. Conversely, the leeward internal Alps experience a reversed orographic effect because the overshoot of the northern crest of the Alps (southern border of the Berner Alps and Limmat catchment areas) brings precipitation in the Rhône and Rhine valleys (northern border of the central Valais and Adula Alps areas), and because a precipitation-shadow effect keeps the southern mountains relatively dry (Foresti et al., 2018). In contrast with winter stratiform precipitation, summer convective precipitation (Fig. 2i and j) develops primarily over the pre-alpine regions of Switzerland (Barton et al., 2020; Nisi et al., 2018), which creates a mid-slope precipitation maximum in the external Alps regions where this landform is pervasive while the inner Alps

remain relatively dry. A notable exception to this mid-slope precipitation maximum is the overshoot of the southern crest of the Adula Alps by convective systems. These convective systems are initiated in Northern Italy (i.e., south of the Adula Alps) when south-westerly wet air masses originating from the Mediterranean Sea reach the Southern Alps. When they overshoot the southern crest of the Adula Alps, these convective precipitations create a strong orographic precipitation enhancement at high elevations in this area (Panziera and Germann, 2010).

When investigating the occurrence statistics of the different precipitation-elevation models in the Swiss Alps (Table 1), it appears that the idealized linear and positive precipitation-elevation relationship mentioned in the introduction is the exception rather than the rule. Indeed, a positive precipitation lapse rate is observed in only 15 % of the cases tested (a case is defined as the precipitation-elevation relationship estimated for a specific target area and seasonal weather type). Orographic precipitation enhancement (i.e., the increase of precipitation with elevation) is nevertheless the prevailing variation pattern and occurs in 47.5 % of cases, but it is mostly non-linear. The second most common variation pattern is the absence of a trend in precipitation as a function of elevation (37.5 % of cases), and also in this configuration, the non-linearity prevails: 12.5 % of all cases have constant precipitation while 23.75 % display a mid-slope precipitation maximum and 1.25 % a mid-slope precipitation minimum. The less frequent variation pattern is a reverse orographic effect (i.e., the decrease of precipitation with elevation) occurring in 15 % of cases, which is the only configuration where linearity prevails: 13.75 % of all cases are decreasing and linear,

Table 1
Frequency of occurrence for the different patterns of variation and linearity behaviors of the precipitation-elevation relationship. The frequencies reported in this table are expressed as a percentage of total cases (80 cases in total, i.e., 5 target areas x 16 seasonal weather types). Numbers in parentheses correspond to the frequency of cases with strong to very strong evidence for the selected hypothesis of linearity. For each case, the schematics exemplify the configurations that are observed in our Swiss Alps dataset (Fig. 2).

Change in precipitation with elevation	Linear Models M1 or M2	Non-linear Models M3, M4 or M5	Total
Increase M2, M3, M4 or M5	15 % (7.5 %)	32.5 % (22.5 %)	47.5 % (30 %)
No trend M1 or M5	12.5 % (7.5 %)	25 % (22.5 %)	37.5 % (30 %)
Decrease M2, M3, M4 or M5	13.75 % (10 %)	1.25 % (0 %)	15 % (10 %)
Total	41.25 % (25 %)	58.75 % (45 %)	100 % (70 %)

and only 1.25 % decreasing and non-linear.

1.4. Concluding remarks

Capitalizing on the good coverage and high accuracy of a radar-rain gauge merged product over the Swiss Alps, we explored the influence of elevation on mean daily precipitation in an area with a complex topography and diverse hydro-climates. The two main outcomes of this analysis are that, for the Swiss Alps (i) the often postulated linear and positive precipitation-elevation relationship is the exception rather than the rule; and (ii) the linearity, magnitude, and sign of the influence of elevation on precipitation vary tremendously in space and time.

When modeling rainfall-runoff responses in complex topography regions, we therefore recommend the use of models enabling both non-linearity and space–time non-stationarity of the elevation-precipitation relationship, in place of fixed-linear precipitation lapse rates which lack the flexibility to capture the diversity of orographic effects occurring in mountains. Moving towards more flexible precipitation-elevation models can have fundamental implications for the comprehension of the hydrological budget of high-altitude catchments where precipitation is typically interpolated or extrapolated, as well as for cryosphere studies where glacier mass balance strongly depends on accurate precipitation estimations.

2. Methods

2.1. Data and study areas

Our analysis is based on the CombiPrecip (CPC) dataset, which is the result of a fusion between radar and rain gauge data processed and maintained by MeteoSwiss (MeteoSwiss, CPC documentation). The radar data used in CPC is derived from a network of five C-band Doppler radars distributed over Switzerland, whose set-up and data processing have been optimized for precipitation measurement in high-elevation areas (Germann et al., 2022). This includes setting up some of the radar antennas near mountain peaks to reduce beam shielding by topography and ground clutter (i.e., the reflection of the radar beam by the ground), implementing an antenna scan strategy that accounts for the local topographic setting, and specific data pre-processing to mitigate ground clutter, beam shielding, and vertical profile reflectivity

Table 2
Environmental features of the five target areas: footprint, number of precipitation gauges, dominant landforms and precipitation regime.

Target area	Footprint	Gauges	Landforms	Precipitations
Berner Alps	3142 km^2	15	Pre-Alps External Alps	Moderate all year round
Limmat catch.	2165 km^2	18	Pre-Alps External Alps	Moderate in winter and fall High in spring and summer
Central Valais	1429 km^2	16	Internal Alps	Low in winter and fall Moderate in spring and summer
Adula Alps	2194 km^2	14	Internal Alps	Low in winter and fall Moderate in spring and summer
Maggia Valley	1701 km^2	9	Pre-Alps	Moderate in winter High in spring, summer and fall (with intense convective storms)

effects. The rain gauge data used in CPC derive from over 250 high-precision automatic rain gauges of the SwissMetNet network (MeteoSwiss, SwissMetNet documentation), predominantly located in lowlands with nevertheless a good coverage of high elevation areas (58 gauges are located at elevations ranging from 1000 m to 1500 m above sea level (a.s.l.), 37 gauges between 1500 m to 2000 m a.s.l., and 27 gauges above 2000 m a.s.l.). Co-kriging with external drift is used to merge radar and gauge data, resulting in an hourly and 1 km resolution product (Sideris et al., 2014). The CPC dataset is available from 2005 until today, but early epochs are affected by changes in the number of operational radars and rain gauges as well as changes in the processing of ground clutter (MeteoSwiss, CPC documentation), therefore we only use data from 2015 to 2023. To further minimize the possibility of biases in the precipitation data we focus our analysis on the areas that are best covered by the radars, and we have therefore excluded all grid cells affected by beam blocking or ground clutter from the analysis (see Fig. S1).

The elevation data we use is the 200-m Swisstopo product MNT25 (Swisstopo, 2004), which we re-gridded at a 1 km resolution to match the resolution of the precipitation dataset. The topography of Switzerland is complex and varied, including two mountain ranges: the Alps (highest altitude 4634 m a.s.l) and the Jura (highest altitude 1679 m a.s.l), and extensive lowlands (ranging between 400 and 800 m a.s.l.). To assess the diversity of precipitation-elevation relationships in space, we focus on five regions that are deemed representative of the hydro-climates of the Swiss Alps (Table 2). These target areas are subsets of the main water catchments of Switzerland and have been delineated to minimize the dispersion of the observed precipitation-elevation scatter plots within each area (see Fig. S2).

The climate is represented by 16 seasonal weather types that depict the main atmospheric configurations above Europe (Yiou et al., 2008). More precisely, the year is first divided into four seasons: winter (DJF), spring (MAM), summer (JJA), and fall (SON), and then each season is further divided into four weather types based on the spatial patterns of the daily mean geopotential height at 500 hPa over Europe (see Fig. S3). The resulting weather types DJF1, MAM1, JJA1 and SON2 can be connected to the negative phase of the North Atlantic Oscillation (NAO-) and tend to bring wet westerly air masses directly above Switzerland; DJF2, MAM2, JJA2 and SON1 can be connected to the positive phase of the North Atlantic Oscillation (NAO+) during which the low-pressure systems transit mostly above Northern Europe and periodically reach Switzerland; JJA4 can be associated with an Atlantic Low regime associated with low-pressure systems above the Northern Atlantic and relatively high pressures over Switzerland along with scattered and often convective precipitation; DJF3, MAM3, and SON4 correspond to an Atlantic Ridge that brings moderately wet northerly to north-westerly air masses over Switzerland; and DJF4, MAM4, JJA3 and SON3 correspond to a Scandinavian Blocking during which Switzerland stands in the southern margin of a high-pressure system leading to generally dry conditions (except from convective precipitation in summer (JJA3) and fall (SON3)). For a more detailed meteorological interpretation of the weather types, see the original classification description (Yiou et al., 2008) and subsequent studies using this classification for climate science applications (e.g., Krouma et al., 2022).

2.2. Investigating the precipitation-elevation relationship

We investigate the relationship between precipitation (*P*, derived from the CPC dataset) and elevation (*E*, derived from the MNT25 dataset) for each weather type and target area separately. We explore the linearity, sign, and magnitude of this relationship by adjusting five competing regression models to the *P-E* observation scatter plot. These models have been chosen within the family of piecewise linear models to allow a simple comparison between models, and have been designed to cover the spectrum of *P-E* relationships ranging from no dependence (M_1) to a two-segment non-linear model (M_5):

(M_1) constant precipitation for all elevations: $P = a_{11}$
(M_2) linear *P-E* model: $P = a_{21} + a_{22} E$
(M_3) constant precipitation until a given elevation (a_{32}) and then linear trend:

$P = a_{31} + a_{33} E\delta_{E \geq a_{32}}$, with δ the Kronecker delta ($\delta_C = 1$ if the condition C is true and $\delta_C = 0$ otherwise)

(M_4) linear trend until a given elevation (a_{43}) and then constant precipitation:

$P = (a_{41} + a_{42}E)\delta_{E \, < \, a43} + (a_{41} + a_{42}a_{43})\delta_{E \, \geq \, a43}$

(M_5) two-segment piecewise linear model with break-point at altitude a_{54}:

$P = (a_{51} + a_{52}E)\delta_{E \, < \, a53} + (a_{51} + a_{52}a_{53} + a_{54}E)\delta_{E \, \geq \, a53}$

where a_{ij} are model parameters that are estimated from the data by maximization of the log-likelihood assuming independent and identically distributed residuals with a normal distribution. Model calibration is performed under the constraint that the elevation of breaking points (parameters a_{32}, a_{43}, and a_{53}) is comprised between 1000 and 2500 m a. s.l. Subsequently, the model that best fits the data is selected by minimizing the Bayesian Information Criterion (BIC) defined by Schwartz (1978) as $BIC = log(n)k - 2log(L)$, where *k* is the number of parameters of the model at hand, *n* is the number of observations, and log(*L*) is the log-likelihood derived from the estimation step. The BIC has been preferred to other information criteria such as the Akaike Information Criterion (AIC) because it strongly penalizes model complexity, and therefore leads to the selection of simple models which in the present case avoids the spurious detection of non-linearity. When a non-linear model ($M_{NL} \in \{M_3, M_4, M_5\}$) is selected by BIC minimization, we assess the level of evidence provided by the data in favor of the non-linear hypothesis by estimating the Bayes Factor (BF; Kass and Raftery, 1995) between the best linear model (M_L; i.e., the model M_1 or M_2 with the smallest BIC) and M_{NL} using the BIC approximation of the Bayes Factor (Faulkenberry, 2018) written as $BF = exp(-0.5(BIC(M_{NL}) - BIC(M_L)))$.

If *log(BF)* is less than 3 we consider that the evidence for non-linearity is weak, if *log(BF)* ranges between 3 and 5 we consider that it is strong, and if *log(BF)* is above 5 we consider that the evidence for non-linearity is very strong (Kass and Raftery, 1995). We apply the same procedure (by simply inverting the indices $_{NL}$ and $_L$) to assess the evidence for linearity in the case where the model with the smallest BIC is linear.

CRediT authorship contribution statement

Lionel Benoit: Conceptualization, Methodology, Data curation, Writing – original draft. **Erwan Koch:** Methodology, Writing – review & editing. **Nadav Peleg:** Methodology, Writing – review & editing. **Gregoire Mariethoz:** Conceptualization, Methodology, Writing – original draft.

Declaration of competing interest

The authors declare that they have no known competing financial interests or personal relationships that could have appeared to influence the work reported in this paper.

Data availability

The CombiPrecip precipitation dataset is available upon request to the Swiss weather agency MeteoSwiss, and the MNT25 elevation dataset is available upon request to the Swiss mapping agency Swisstopo. The weather type dataset is available online: https://a2c2.lsce.ipsl.fr/index.php/deliverables/102-continuous-time-weather-regimes.

Data pre-processing and statistical analyses have been performed using MATLAB scripts written by the authors, which are available upon request to lionel.benoit@inrae.fr.

Acknowledgments

Appendix A. Supplementary data

Supplementary data to this article can be found online at https://doi.org/10.1016/j.hydroa.2024.100186.

References

Barton, Y., Sideris, I.V., Raupach, T.H., Gabella, M., Germann, U., Martius, O., 2020. A multi-year assessment of sub-hourly gridded precipitation for Switzerland based on a blended radar—rain-gauge dataset. Int. J. Climatol. 40 (12), 5208–5222.

Benoit, L., Lucas, M., Tseng, H., Huang, Y.F., Tsang, Y.P., Nugent, A.D., Giambelluca, T.W., Mariethoz, G., 2021. High space-time resolution observation of extreme orographic rain gradients in a Pacific Island catchment. Front. Earth Sci. 8.

Benoit, L., Sichoix, L., 2023. Sub-daily rainfall patterns in the mountainous regions of the Island of Tahiti: insights from a one-year rain gauge network expansion. J. Hydrol.: Reg. Stud. 50, 101559.

Bohne, L., Strong, C., Steenburgh, W.J., 2020. Climatology of orographic precipitation gradients in the contiguous Western United States. J. Hydrometeorol. 21 (8), 1723–1740.

Collados-Lara, A.-J., Pardo-Igúzquiza, E., Pulido-Velazquez, D., Jiménez-Sánchez, J., 2018. Precipitation fields in an alpine Mediterranean catchment: inversion of precipitation gradient with elevation or undercatch of snowfall? Int. J. Climatol. 38 (9), 3565–3578.

Dallan, E., Marra, F., Fosser, G., Marani, M., Formetta, G., Schär, C., Borga, M., 2023. How well does a convection-permitting regional climate model represent the reverse orographic effect of extreme hourly precipitation? Hydrol. Earth Syst. Sci. 27 (5), 1133–1149.

Daly, C., Neilson, R.P., Phillips, D.L., 1994. A statistical-topographic model for mapping climatological precipitation over mountainous terrain. J. Appl. Meteorol. Climatol. 33 (2), 140–158.

Dura, V., Evin, G., Favre, A.C., Penot, D., 2024. Spatial variability of seasonal precipitation lapse rates in complex topographical regions–application in France. Egusphere 2024, 1–34.

Faulkenberry, T.J., 2018. Computing Bayes factors to measure evidence from experiments: an extension of the BIC approximation. Biometr. Lett. 55 (1), 31–43.

Foresti, L., Pozdnoukhov, A., 2012. Exploration of alpine orographic precipitation patterns with radar image processing and clustering techniques. Meteorol. Appl. 19, 407–419.

Foresti, L., Sideris, I.V., Panziera, L., Nerini, D., Germann, U., 2018. A 10-year radar-based analysis of orographic precipitation growth and decay patterns over the Swiss Alpine region. Q. J. R. Meteorolog. Soc. 144 (716), 2277–2301.

Garavaglia, F., Le Lay, M., Gottardi, F., Garçon, R., Gailhard, J., Paquet, E., Mathevet, T., 2017. Impact of model structure on flow simulation and hydrological realism: from a lumped to a semi-distributed approach. Hydrol. Earth Syst. Sci. 21 (8), 3937–3952.

Germann, U., Boscacci, M., Clementi, L., Gabella, M., Hering, A., Sartori, M., et al., 2022. Weather radar in complex orography. Remote Sens. (Basel) 14 (3), 503.

Giambelluca, T.W., Chen, Q., Frazier, A.G., Price, J.P., Chen, Y.-L., Chu, P.-S., Eischeid, J. K., Delparte, D.M., 2013. Online rainfall atlas of Hawai'i. Bull. Am. Meteorol. Soc. 94, 313–316.

Houze, R.A., 2012. Orographic effects on precipitating clouds. Rev. Geophys. 50, RG000365.

Isotta, F.A., Frei, C., Weilguni, V., Perčec Tadić, M., Lassegues, P., Rudolf, B., et al., 2014. The climate of daily precipitation in the Alps: development and analysis of a high-resolution grid dataset from pan-Alpine rain-gauge data. Int. J. Climatol. 34 (5), 1657–1675.

Kass, R.E., Raftery, A.E., 1995. Bayes factors. J. Am. Stat. Assoc. 90 (430), 773–795.

Krouma, M., Yiou, P., Déandreis, C., Thao, S., 2022. Assessment of stochastic weather forecast of precipitation near European cities, based on analogs of circulation. Geosci. Model Dev. 15 (12), 4941–4958.

Longman, R.J., Timm, O.E., Giambelluca, T.W., Kaiser, L., 2021. A 20-year analysis of disturbance-driven rainfall on O'ahu, Hawai'i. Mon. Weather Rev. 149 (6), 1767–1783.

Markstrom, S.L., Regan, R.S., Hay, L.E., Viger, R.J., Webb, R.M., Payn, R.A., LaFontaine, J.H., 2015. PRMS-IV, the Precipitation-Runoff Modeling System, Version 4, Tech. Rep., U.S. Geological Survey Techniques and Methods. doi: 10.3133/tm6B7.

Marra, F., Armon, M., Morin, E., 2022. Coastal and orographic effects on extreme precipitation revealed by weather radar observations. Hydrol. Earth Syst. Sci. 26 (5), 1439–1458.

Masson, D., Frei, C., 2014. Spatial analysis of precipitation in a high-mountain region: exploring methods with multi-scale topographic predictors and circulation types. Hydrol. Earth Syst. Sci. 18 (11), 4543–4563.

MeteoSwiss. (CPC documentation). Hourly Precipitation Estimation through Rain-Gauge and Radar: CombiPrecip, Documentation of MeteoSwiss Grid-Data Products, available online: https://www.meteoswiss.admin.ch/jcr:2691db4e-7253-41c6-a413-2c75c9de11e3/ProdDoc_CPC.pdf (last access 2024/08/02).

MeteoSwiss (SwissMetNet documentation). SwissMetNet: The MeteoSwiss reference monitoring network, available online: https://www.meteoswiss.admin.ch/dam/jcr:b24af19f-c32f-464d-b2c4-163c72c8f071/SwissMetNetTheMeteoSwissReferenceMonitoringNetwork.pdf (last access 2024/08/02).

Michelon, A., Benoit, L., Beria, H., Ceperley, N., Schaefli, B., 2021. Benefits from high-density rain gauge observations for hydrological response analysis in a small alpine catchment. Hydrol. Earth Syst. Sci. 25, 2301–2325.

Nisi, L., Hering, A., Germann, U., Martius, O., 2018. A 15-year hail streak climatology for the Alpine region. Q. J. R. Meteorolog. Soc. 144 (714), 1429–1449.

Panziera, L., Germann, U., 2010. The relation between airflow and orographic precipitation on the southern side of the Alps as revealed by weather radar. Q. J. R. Meteorolog. Soc. 136 (646), 222–238.

Panziera, L., Gabella, M., Germann, U., Martius, O., 2018. A 12-year radar-based climatology of daily and sub-daily extreme precipitation over the Swiss Alps. Int. J. Climatol. 38 (10), 3749–3769.

Roe, G.H., 2005. Orographic precipitation. Ann. Rev. Earth Planet. Sci. 33, 645–671.

Schwartz, G., 1978. Estimating the dimension of a model. Ann. Stat. 6, 461–464.

Sideris, I.V., Gabella, M., Erdin, R., Germann, U., 2014. Real-time radar-rain-gauge merging using spatio-temporal co-kriging with external drift in the alpine terrain of Switzerland. Q. J. R. Meteorolog. Soc. 140 (680), 1097–1111.

Siler, N., Roe, G., Durran, D., 2013. On the dynamical causes of variability in the rain-shadow effect: a case study of the Washington Cascades. J. Hydrometeorol. 14 (1), 122–139.

Swisstopo, 2004. DHM25: The digital height model of Switzerland, Federal office of topography – product information, available online: https://backend.swisstopo.admin.ch/fileservice/sdweb-docs-prod-swisstopoch-files/files/2023/11/14/c4f59d00-5935-4de3-88dc-fa699bf685ea.pdf (last access 2024/04/05).

Yiou, P., Goubanova, K., Li, Z.X., Nogaj, M., 2008. Weather regime dependence of extreme value statistics for summer temperature and precipitation. Nonlinear Processes Geophys. 15 (3), 365–378.

Lionel Benoit[a], Erwan Koch[b], Nadav Peleg[b,c], Gregoire Mariethoz[b,c,*]

[a] *Biostatistics and Spatial Processes, INRAE, Avignon, France*

[b] *Expertise Center for Climate Extremes (ECCE), Faculty of Business and Economics (HEC) and Faculty of Geosciences and Environment, University of Lausanne, Lausanne, Switzerland*

[c] *Institute of Earth Surface Dynamics, University of Lausanne, Lausanne, Switzerland*

[*] Corresponding author.
E-mail address: gregoire.mariethoz@unil.ch (G. Mariethoz).